〈Technical Note〉

A SIMPLE ANALYTICAL METHOD FOR NONLINEAR DENSITY WAVE TWO-PHASE INSTABILITY IN A SODIUM-HEATED AND HELICALLY COILED STEAM GENERATOR

SEONG-O KIM*, SEOK-KI CHOI and HAN-OK KANG
Korea Atomic Energy Research Institute, Fast Reactor Development Division
1045 Daedeokdaero, Yuseong, Daejeon, 305-353, Korea
*Corresponding author. E-mail : sokim@kaeri.re.kr

Received October 2, 2008
Accepted for Publication February 11, 2009

A simple model to analyze non-linear density-wave instability in a sodium-cooled helically coiled steam generator is developed. The model is formulated with three regions with moving boundaries. The homogeneous equilibrium flow model is used for the two-phase region and the shell-side energy conservation is also considered for the heat flux variation in each region. The proposed model is applied to the analysis of two-phase instability in a JAEA (Japan Atomic Energy Agency) 50MWt No.2 steam generator. The steady state results show that the proposed model accurately predicts the six cases of operating temperatures on the primary and secondary sides. The sizes of three regions, the secondary side pressure drop according to the flow rate, and the temperature variation in the vertical direction are also predicted well. The temporal variations of the inlet flow rate according to the throttling coefficient, the boiling and superheating boundaries and the pressure drop in the two-phase and superheating regions are obtained from the unsteady analysis.

KEYWORDS : Two-Phase Flow, Density Wave Instability, Helically Coiled Once-through Steam Generator, Sodium Cooled Fast Reactor

1. INTRODUCTION

Once-through steam generators are advantageous because they are compact and produce superheated steam without an additional steam separator. Particularly, the use of helical coils offers compactness and structural stability and enhances the heat transfer due to the centrifugal force. Due to these advantages, sodium-cooled fast reactors, for example the KALIMER-600 (Korea Advanced Liquid Metal Reactor-600MWe) under development at KAERI (Korea Atomic Energy Research Institute), utilize a once-through helically coiled steam generator to produce steam. However, these steam generators are associated with two-phase flow instability on the tube side. Flow instability on the tube side can lead to flow oscillation, which disturbs the control system and causes mechanical damage. Thus, understanding and predicting the potential for flow instability on the tube side is very important in the design of steam generators in sodium-cooled fast reactors.

Two types of flow instabilities have been observed in helically coiled steam generators. The first type is a flow excursion type known as Ledinegg instability, which is a static instability. The second type is density wave instability, which is a self-sustaining instability. Ledinegg instability can occur only if the static tube pressure drop versus the mass flow rate curve has a negative slope. Density wave instability has been investigated vigorously with regard to the safe operation of BWRs (Boiling Water Reactors). Kakac and Liu [1] and Boure et al. [2] offer a detailed description of flow instability in BWRs and once-through steam generators. There are a few experimental studies on density wave instability in steam generators related to the development of sodium-cooled fast reactors. Waszink and Efferding [3] and Unal [4-6] conducted experiments with sodium-heated steam generators. The works by Sano et al. [7], Tsuchiya et al. [8], Kubota et al. [9] and Manabe et al. [10] report the operating experiences of actual steam generators. These works are particularly valuable because they provide experimental data for the validation of computer analysis codes.

In the present work, a non-linear calculation method of the density-wave instability on the secondary side of a sodium-cooled fast reactor steam generator is developed. The method is formulated with three regions (the sub-cooled, boiling and post-dryout regions) with moving boundaries. It is applied to the analysis of the density-wave instability in the JAEA 50MWt No. 2 steam generator, where the operating experiences are reported in Kubota et al. [9] and Manabe et al. [10]. The computed results are compared with experimental data, and a number of important parameters from steady and unsteady computations are explained.

2. GOVERNING EQUATIONS AND NUMERICAL METHOD

There are a number of tubes having common pressure headers at both ends of a steam generator. Basically, all tubes should be modeled to analyze flow instability, but such a scheme brings forth so many degrees of freedom to the extent that it becomes difficult to formulate adequate governing equations. This difficulty is overcome in experiments here through the use of only 3 ~ 5 tubes or a single tube with an additional bypass line. It is known from former studies that when dozens of tubes have common headers at both ends, the effect of other tubes can be approximately substituted to a constant pressure drop condition. This assumption is adopted in this study. Other assumptions are as follows:

(a) The heat flux in the steam generators is generally much lower than that of BWR cores and the nucleate boiling point in the tube is nearly identical to the bulk saturation point. In addition, as the pressure drop in the sub-cooled region excluding the inlet orifice only accounts for an insignificant share of the total pressure drop in the tube, sub-cooled nucleate boiling is not considered. Thermal equilibrium between the two phases in the boiling region is assumed in this study.

(b) The primary fluid is well mixed and has a high heat capacity. Additionally, the effects of each tube on the shell side are overlapped with different phase angles, and the primary temperature can be assumed to be time-invariant.

(c) The tube wall heat capacity is neglected. It was evident through simple time-scale analysis that the time scale related to tube wall dynamics is very short relative to the residence time in the tube.

Fig. 1 shows the computational domain and the definitions of the parameters used in this study. The domain includes both primary and secondary sides. The secondary side is composed of the sub-cooled, boiling

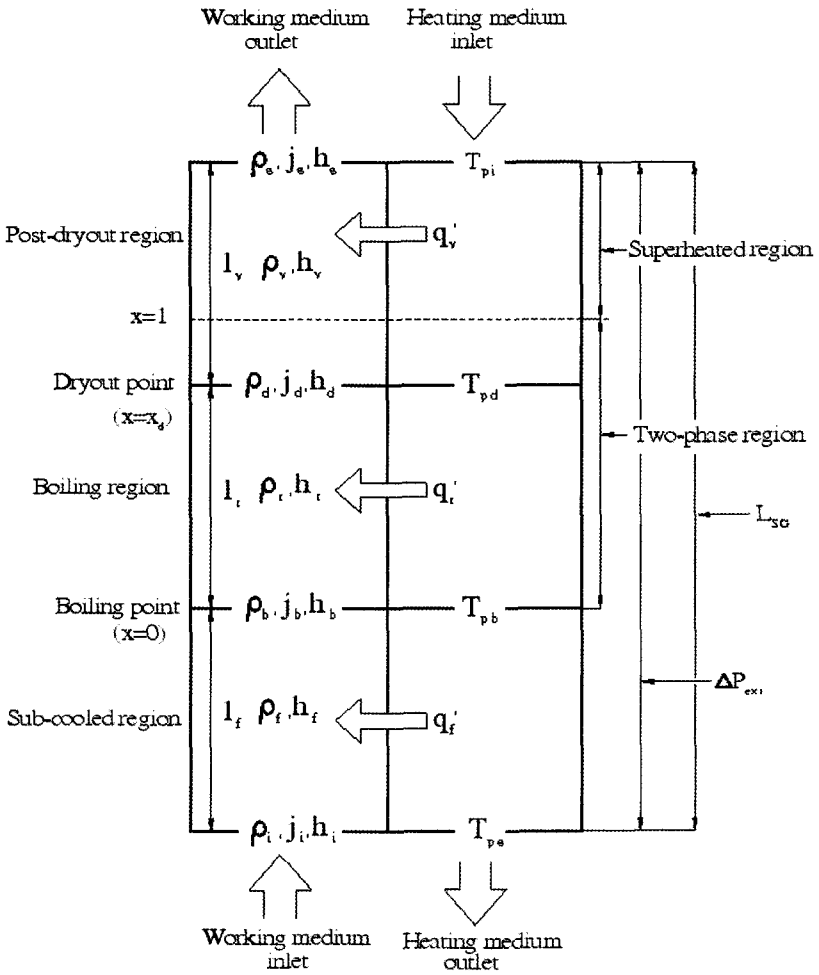

Fig. 1. Calculation Domain and Parameters

and post-dryout regions. The boiling region begins at the boiling point and ends at the dryout point. The post-dryout region is composed of mist and pure vapor flow regions. As the mist flow region comprises only a small portion of the post-dryout region and because the thermo-hydraulic characteristics of the mist and pure vapor flow regions do not differ greatly, the two regions are treated as one post-dryout region. The heat fluxes in each region are calculated from the log-mean temperature differences. The overall secondary pressure drop is held constant. The length scale of the secondary side is the total tube length L_{SG} while that of the primary side is H_{SG}. Detailed derivation of the governing equations is given in Kang et al. [11]; only a brief description of this is given here.

2.1 Primary Side

The primary fluid temperature distribution is needed for the time-varying heat flux. Simplified steady energy conservation equations are utilized for this purpose,

$$\dot{m}_p(C_{pi}T_{pi} - C_{pd}T_{pd}) = q''_{vo}\xi_p l_v \tag{1}$$

$$\dot{m}_p(C_{pd}T_{pd} - C_{pb}T_{pb}) = q''_{to}\xi_p l_t \tag{2}$$

$$\dot{m}_p(C_{pb}T_{pb} - C_{pe}T_{pe}) = q''_{fo}\xi_p l_f \tag{3}$$

where ξ_p is the wetted perimeter on the primary side and the l_v, l_t, l_f are the lengths of the tubes in each region. The heat fluxes in the above equation are calculated by the following equations:

$$q''_{fo} = h_{fo}\frac{(T_{ep} - T_{is}) - (T_{bp} - T_{bs})}{\ln[(T_{ep} - T_{is})/(T_{bp} - T_{bs})]} \tag{4}$$

$$q''_{to} = h_{to}\frac{(T_{bp} - T_{bs}) - (T_{dp} - T_{ds})}{\ln[(T_{bp} - T_{bs})/(T_{dp} - T_{ds})]} \tag{5}$$

$$q''_{vo} = h_{vo}\frac{(T_{ip} - T_{es}) - (T_{dp} - T_{ds})}{\ln[(T_{ip} - T_{es})/(T_{dp} - T_{ds})]} \tag{6}$$

The heat transfer coefficients in above equations are computed as follows:

$$\frac{1}{h} = \frac{1}{h_s}\frac{D_o}{D_i} + \frac{D_o}{2k_w}\ln\frac{D_o}{D_i} + \frac{1}{h_p} \tag{7}$$

2.2 Secondary Side

The mass and energy conservation equations in each region of the secondary side can be expressed as shown below.

Sub-cooled region:

$$\rho_f \frac{d}{dt}(l_f) = \rho_i j_i - \rho_b j_b \tag{8}$$

$$\rho_f \frac{d}{dt}(l_f h_f) = \rho_i j_i h_i - \rho_b j_b h_b + \frac{q''_f \xi_s l_f}{A_s} \tag{9}$$

Boiling region:

$$\rho_t \frac{d}{dt}(l_t) = \rho_b j_b - \rho_d j_d \tag{10}$$

$$\rho_t \frac{d}{dt}(l_t h_t) = \rho_b j_b h_b - \rho_d j_d h_d + \frac{q''_t \xi_s l_t}{A_s} \tag{11}$$

Post-dryout region:

$$\rho_v \frac{d}{dt}(l_v) = \rho_d j_d - \rho_e j_e \tag{12}$$

$$\rho_v \frac{d}{dt}(l_v h_v) = \rho_d j_d h_d - \rho_e j_e h_e + \frac{q''_v \xi_s l_v}{A_s} \tag{13}$$

The momentum conservation equation is set up over the entire tube length, as follows:

$$\Delta P_{ext} = \frac{d(\rho_f j_f)}{dt}l_f + \frac{d(\rho_t j_t)}{dt}l_t + \frac{d(\rho_v j_v)}{dt}l_v + \rho_e j_e^2 - \rho_i j_i^2 + g(\rho_f l'_f + \rho_t l'_t + \rho_v l'_v) + \frac{\xi_s}{A_s}(\tau_{wf} l_f + \tau_{wt} l_t + \tau_{wv} l_v) + \frac{1}{2}k_i \rho_i j_i^2 \tag{14}$$

While the velocities relative to moving boundaries are used in the mass and energy equations, the absolute velocities are given in the momentum equation. The following relations between the two velocities can be applied:

$$j'_b = j_b + \frac{dl_f}{dt} \tag{15}$$

$$j'_d = j_d + \frac{dl_f}{dt} + \frac{dl_t}{dt} \tag{16}$$

By manipulation of the above equations, one can obtain the following relations:

$$j_b = -\frac{\rho_i}{\rho_b} j_i + 2\frac{q''_f \xi_s l_f}{A_s h_{bi} \rho_b} \tag{17}$$

$$j_d = \frac{\rho_i}{\rho_d} j_i - 2\frac{q''_f \xi_s l_f}{A_s h_{bi} \rho_d} + 2\frac{q''_t \xi_s l_t}{A_s h_{db} \rho_d} \tag{18}$$

If Eqs.(17) and (18) are inserted in Eqs.(8) and (10), the equations for the l_f, l_t values are obtained. The momentum equation, Eq.(14), can then be written in following forms:

$$\frac{dl_f(t)}{dt} = a_1 j_i(t) + a_2 l_f(t) \tag{19}$$

$$\frac{dl_t(t)}{dt} = a_3 j_i(t) + a_4 l_f(t) + a_5 l_t(t) \tag{20}$$

$$a_6 \frac{dj_i(t)}{dt} = \Delta P_{ext} - \Delta P_f - \Delta P_t - \Delta P_v - \Delta P_{tran} \tag{21}$$

Details of the constants and pressure differences in Eq.(19) to Eq.(21) are given in Kang et al. [11] and are not reproduced here. In order to solve Eqs.(19)-(21) the correlations are needed to compute the heat transfer coefficient and friction factor. The correlation by Kalish and Dwyer [12] is used for the heat transfer coefficient on the primary side. On the secondary side, the correlation reported in the Mori and Nakayma [13] is used for the heat transfer in the single-phase regions, while that by Schrock and Grossman [14] is used in the two-phase region. For the friction factor on the secondary side, the correlation by Ito [15] is used in the single-phase region while that by Kozeki [16] is used in the two-phase region.

The transient calculations begin from steady values that are obtained from steady state calculations. The calculation is done by use of the IMSL DIVPRK subroutine, which uses the Runge-Kutta-Verner sixth-order solution algorithm. The phase boundary oscillates during the transient calculation. The primary temperatures at the interface are obtained from the steady state solution assuming the existence of linear temperature profiles in each region.

3. RESULTS AND DISCUSSION

The simple calculation method described in the previous section was applied to the analysis of the density-wave instability in the JAEA 50MWt No. 2 steam generator, where the operating experiences are reported in Kubota et al. [9] and Manabe et al. [10]. Table 1 shows the design data and operating conditions of the JAEA 50MWt No. 2 steam generator.

Initially shown are the steady state results in which the throttling coefficient in the inlet orifice is very large so that there is no temporal oscillation. Fig. 2 shows a comparison of the predicted steady state exit temperatures of the primary and secondary sides with the measured data for six test operation cases. It was observed that the predicted temperatures agree well with the experimental data, showing that the present calculation method is reliable. The present code was also validated by Kang et al. [17] for the experiment of Nariai [18], which also showed that the present code suitably predicts the threshold inlet throttling coefficient and the oscillation period. Fig. 3 shows the lengths of the sub-cooled, two-phase and

Table 1. Design Data and Operating Conditions of the JAEA 50MWt No. 2 Steam Generator

Parameter	Unit	
Rated Full Power	MWt	40.2
Type of Tubes		Helical Coil
Heat Transfer Area	m^2	237
Number of Tubes		33
Outer Diameter of Tube	mm	31.8
Wall Thickness (Nominal)	mm	3.8
Number of Coils		6
Coil Diameter (Minimum/Maximum)	mm	780/1280
Effective Tube Length	m	68.1
Tube Material		2.1/4Cr-1Mo
Inlet Temperature of Sodium	°C	476
Outlet Temperature of Sodium	°C	320
Sodium Flow rate	kg/s	201
Inlet Temperature of Water/Steam	°C	240
Outlet Temperature Steam	°C	366
Outlet Pressure of steam	MPa	13.9
Water Flow Rate	kg/s	22.1

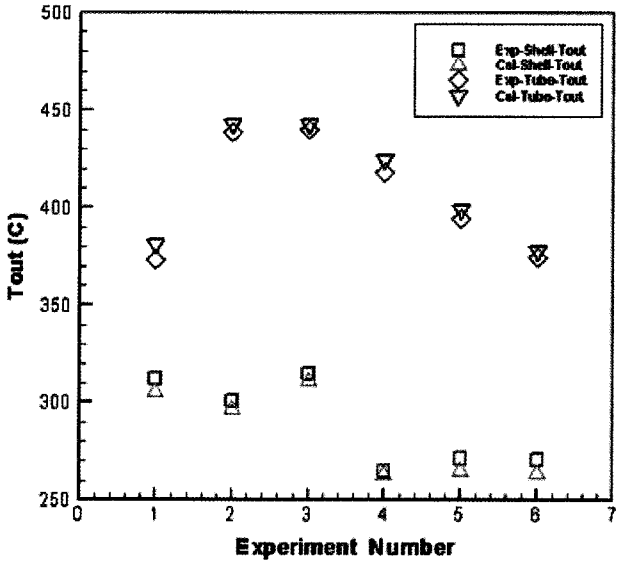

Fig. 2. The Predicted Primary and Secondary Exit Temperatures with the Experimental Data

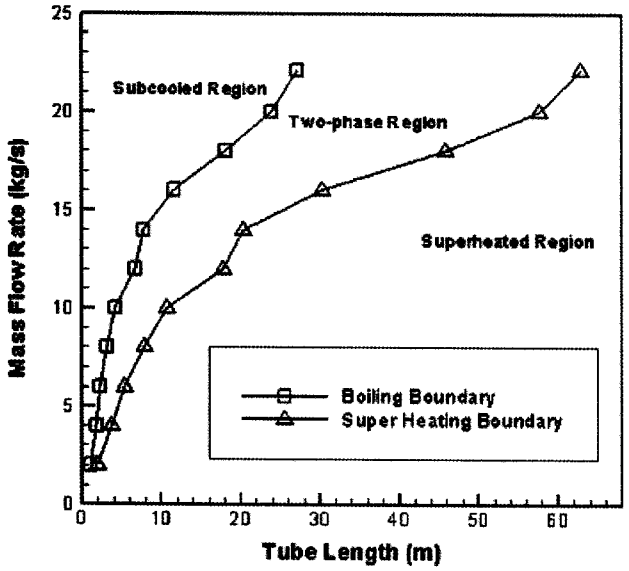

Fig. 3. The Lengths of the Three Regions According to the Mass Flow Rate

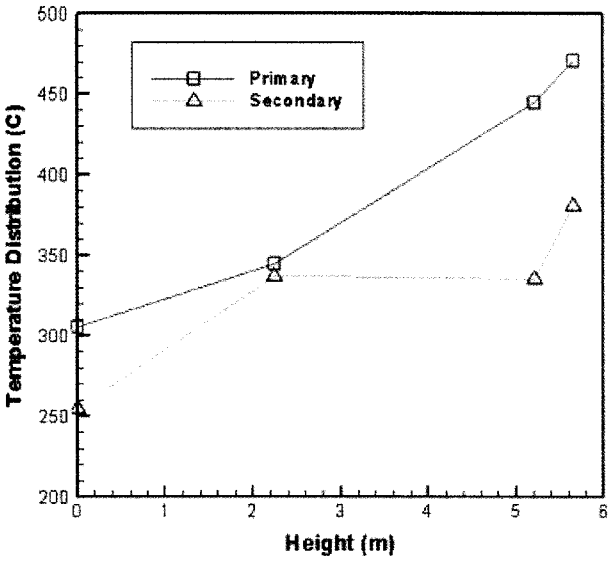

Fig. 5. The Primary and Secondary Temperature Distributions in the Vertical Direction

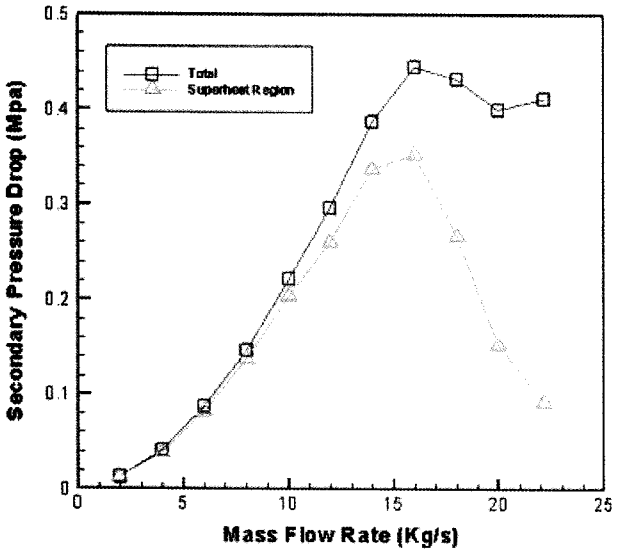

Fig. 4. The Pressure Drop on the Secondary Side According to the Mass Flow Rate

superheated regions according to the magnitude of the inlet mass flow rate on the secondary side. When the inlet mass flow rate is small, most of the tube length is filled with superheated vapor. If the inlet mass flow rate is increased, the lengths of the sub-cooled and two-phase regions increase rapidly. Under actual operation, the mass flow rate on the secondary side is approximately 22 kg/sec; thus, the length of the superheated region is very short. Fig. 4 shows the pressure drop over the entire secondary side together with that in the superheated region. It is clear that the pressure drop in the superheated region is dominant when the mass flow rate is less than 16kg/sec. The figure also shows that the pressure drops on the secondary side and that in the superheated region reach their maximum values when the mass flow rate is approximately 16kg/s. The figure shows that the pressure drop in the superheated region diminished suddenly when the mass flow rate exceeded 16kg/sec; however, the pressure drop on the entire secondary side decreased slightly and began to increase when the mass flow rate approached 20kg/s. Ledinegg instability can occur only if the static tube pressure drop versus the mass flow rate curve has a negative slope. This phenomenon can occur when the mass flow rate is between 15kg/s and 20kg/s. Fig. 5 shows the temperature distribution on both the primary and secondary sides in the vertical direction. The temperature on the primary side has its maximum value at the top and decreases as the primary fluid flows in the downward direction due to the heat transfer to the secondary side. The temperature on the secondary side increases rapidly in the sub-cooled region, is nearly constant in the two-phase region, and increases rapidly in the superheated region. This type of temperature variation is well known, with most books on thermodynamics covering it in depth.

This section presents the computed results from the unsteady calculation. Fig. 6 shows the temporal variation of the inlet mass flow rate according to the magnitude of the throttling coefficient of the inlet orifice. A case of operations in which the secondary mass flow rate is 8.54kg/s and the primary mass flow rate is 11.85kg/s was chosen. If an inlet orifice does not exist (Ki=0), the flow is unstable and the inlet mass flow rate oscillates severely. The magnitude of oscillation becomes smaller if the throttling

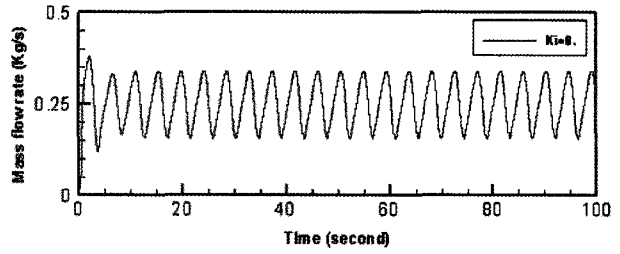

(a) Ki=0.0

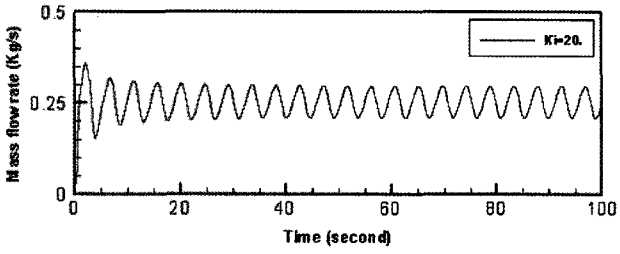

(b) Ki=20

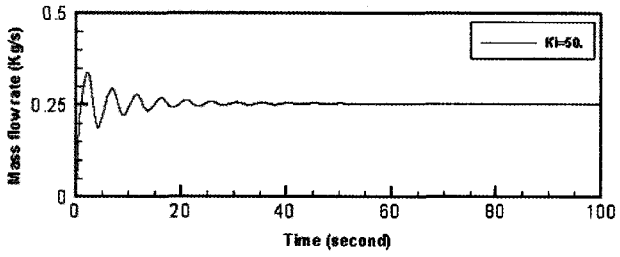

(c) Ki=50

Fig. 6. The Temporal Variation of the Inlet Mass Flow Rate According to the Throttling Coefficient

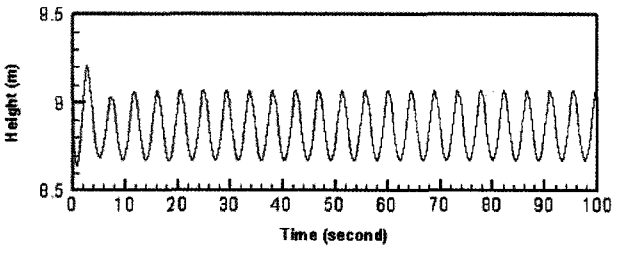

(a) Temporal variation of the boiling boundary

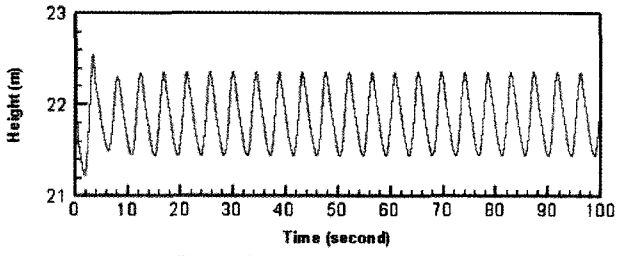

(b) Temporal variation of the superheating boundary

Fig. 7. The Temporal Variations of the Boiling and Superheating Boundaries

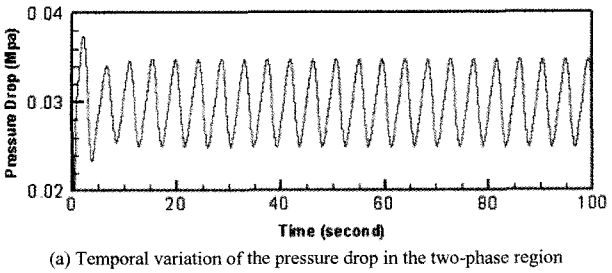

(a) Temporal variation of the pressure drop in the two-phase region

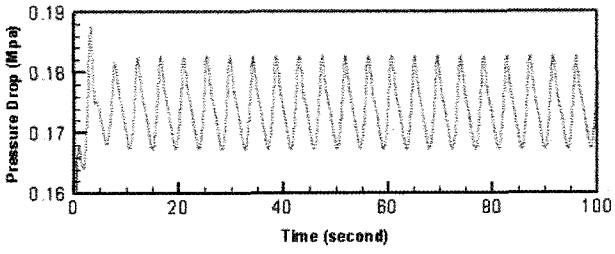

(b) Temporal variation of the pressure drop in the superheating region

Fig. 8. Temporal Variations of the Pressure Drop in the Two-phase and Superheating Regions

coefficient becomes larger (Ki=20). When the throttling coefficient is increased further (Ki=50), the temporal oscillation of the inlet mass flow rate becomes constant. Fig. 7 shows the temporal oscillation of boiling and superheating boundaries when the inlet orifice does not exist (Ki=0.). The frequency of the oscillation is nearly identical while the amplitude of the oscillation for the superheating boundary is larger than that of the boiling boundary. The same phenomenon is also observed in Fig. 8, which shows the temporal oscillations during pressure drops in the two-phase and superheating regions. These behaviors differ depending on the operating condition. Here, the results of only one operating condition are reported. The results of these types of investigations may provide the magnitude of the throttling coefficient for the inlet orifice in actual steam generators with which density-wave oscillation can be avoided.

4. CONCLUSIONS

A simple model to analyze the non-linear density-wave instability in a sodium-cooled helically coiled steam generator is developed. The proposed model is applied to the analysis of two-phase instability in a JAEA 50MWt No. 2 steam generator. The steady state results show that the proposed model accurately predicts six cases of operating temperatures on the primary and secondary sides. From the unsteady results, the effects of the magnitude of the throttling coefficient on the flow oscillation are investigated. The findings of this study provide the magnitude of throttling coefficient of the

inlet orifice for an existing steam generator in the KALIMER-600 under development at KAERI.

ACKNOWLEDGEMENT

This study was supported by the Nuclear Research and Development Program of the Ministry of Education, Science and Technology of Korea.

NOMENCLATURE

Notation

A	area
a,b	constants in Eqs.(19)-(21)
C_p	heat capacity
D_i	inner diameter of tube
D_o	outer diameter of tube
g	gravity
h	heat transfer coefficient or enthalpy
j	velocity
j'	real velocity defined in Eqs.(15)-(16)
k	thermal conductivity
Ki	inlet orifice throttling coefficient
l	length of each region
l'	defined as $l' = l\frac{H_{SG}}{L_{SG}}$
$\dot{m}$	mass flow rate
P	pressure
q''	heat per unit area
t	time
T	temperature

Greek

ξ_p	wetted perimeter
ρ	density
τ_w	wall friction

Subscripts

b	boiling point
bi	difference between inlet and boiling points
d	dryout point
db	difference between boiling and dryout points
e	exit
ext	external
i	inlet
f	friction or sub-cooled region average value
o	outer
p	primary
r	reference
SG	steam generator
s	secondary
sys	system
t	two-phase region average value
$tran$	transient
v	superheated region average value
w	tube wall
0	steady state value.

REFERENCES

[1] S. Kakac, and H. T. Liu, "Two-Phase Flow Dynamic Instabilities in Boiling System," *Multiphase Flow and Heat Transfer*, pp.403-444, (1991).

[2] J. A. Boure, A. E. Bergles and L. S. Tong, "Review of Two-Phase Flow Instability," *Nuclear Engineering and Design*, Vol.25, pp. 165-192, (1973).

[3] R. P. Waszink, and L. E. Efferding, "Hydrodynamic Stability and Thermal Performance Test of a 1-MWt Sodium Heated Once-Through Steam Generator Model," *ASME paper 73-PWR-16* (1973).

[4] H. C. Unal, M. L. G. van Gasselt, and P. W. P. H. Ludwig, "Dynamic Instabilities in Tubes of a Large Capacity, Straight-Tube, Once-Through Sodium Heated Steam Generator," *Int. J. Heat Mass Transfer*, Vol. 20, pp.1389-1398, (1977).

[5] H. C. Unal, "Correlations for the Determination of the Inception Conditions of Density-Wave Oscillations for Forced and Natural Circulation Steam Generator Tubes, *Trans. ASME J. Heat Transfer*, Vol. 102, pp. 14-19, (1980).

[6] H. C. Unal, "Density-Wave Oscillations in Sodium Heated Once-Through Steam Generator Tubes," *Trans. ASME J. Heat Transfer*, Vol. 103, pp. 485-491.

[7] A. Sano, A. Kanamori, T. Tsuchiya and H. Yamashita, "1-MWt Steam Generator Operating Experience," *ASME-paper 73-HT-53*, (1973).

[8] T. Tsuchiya, J. Kubota, T. Takeuchi and T. Takemura, "Hydrodynamic Stability Tests for LMFBR Sodium Heated Steam Generators," *Proceedings of Japan-US Seminar on Two-Phase Flow Dynamics*, pp. 399-414, (1979).

[9] J. Kubota and T. Tsuchiya, "Hydrodynamic Stability Tests and Analytical Model Development for Once-Through Sodium Heated Steam Generator," *Boiler Dynamic and Control in Nuclear Power Stations*, pp. 105-115, (1979).

[10] F. Manabe, T. Kosugi, T. Tsuchiya and J. Endo, "Experimental Studies of Heat Transfer Performance with the NO.2 50MW Steam Generator in Japan," *The Topical Meeting on R&D Fabrication and Operating Experience on Steam Generators for LMFBR's*, (1981).

[11] H. O. Kang et al., *Analysis of Once-Through Steam Generator Instability*, KAERI Report, KAERI/TR-1068, (1998).

[12] S. Kalish, and O. E. Dwyer, "Heat Transfer to NaK Flow through Unbaffled Rod Bundle," *Int. J. Heat and Mass Transfer*, Vol.10, pp. 1533-1558, (1967).

[13] Y. Mori, and W. Nakayama, "Study on Forced Convective Heat Transfer in Curved Pipes," *Int. J. Heat and Mass Transfer*, Vol.10, pp.37-59, (1967).

[14] V. E. Schrock and L. F. Grossman, *Forced Convection Boiling Studies*, The University of California Berkeley, Report no.73308-UCX-2182, (1959).

[15] H. Ito, "Friction Factors for Turbulent Flow in Curved Pipes," *Trans. ASME J. Basic Eng.* Vol. 81, pp. 123-134, (1959).

[16] M. Kozeki, H. Nariai, T. Furukawa and K. Kurosu, "A Study of Helically-Coiled Tube Once-Through Steam Generator," *Bulletin of the JSME*, Vol.13, pp. 1485-1494, (1970).

[17] H. K. Kang, H. Y. Kim, J. H. Yoon, J. P. Kim and D. J. Lee, "Development of Simple Analytical Model for Helical Once Through Steam Generator Instability,' *Ninth International Topical Meeting on Nuclear Reactor Thermal Hydraulics* (*NURETH-9*), San Francisco,

California, October 3-8, (1999).
[18] H. Nariai , "Friction Pressure Drop and Heat Transfer Coefficient of Two-Phase Flow in the Helically Coiled Tube Once-Through Steam Generator for Integrated Type Marine Water Reactor, *J. Nuc. Sci. Tec.* Vol.19(11), pp. 936~947, 1982.